Systematic study of the Woods-Saxon potential parameters between heavy-ions*

Lin Gan(甘林)[1] Zhi-Hong Li(李志宏)[2,3†] Hui-Bin Sun(孙慧斌)[4‡] Shi-Peng Hu(胡世鹏)[4]
Er-Tao Li(李二涛)[4] Jian Zhong(钟健)[4]

[1]Key Laboratory of Optoelectronic Devices and Systems of Ministry of Education and Guangdong Province, College of Optoelectronic Engineering, Shenzhen University, Shenzhen 518060, China
[2]China Institute of Atomic Energy, Beijing 102413, China
[3]School of Nuclear Science and Technology, University of Chinese Academy of Sciences, Beijing 101408, China
[4]College of Physics and Optoelectronic Engineering, Shenzhen University, Shenzhen 518060, China

Abstract: Experimental elastic scattering angular distributions of ^{11}B, ^{12}C, and ^{16}O + heavy-ions are used to study the Woods-Saxon potential parameters. Best fitted values of the diffuseness parameters are found for each system, and a linear relationship is expressed between the diffuseness parameters and $A_1^{1/3}+A_2^{1/3}$. The correlation of the potential depth and radius parameters with $A_1^{1/3}+A_2^{1/3}$ is also revealed within the limitations of the diffuseness parameter formula. Because the incident energies of most of the analyzed reactions are below or around the Coulomb barrier, the energy dispersion relation between the real and imaginary potentials is considered in order to investigate the ratio between the imaginary and real potential well depths, resulting in an expression of W/V. Within the limitation of the volume integrals calculated with the Sã o Paulo potential, parameterized formulas for the depth and radius parameters are obtained. The systematic Woods-Saxon potential parameters derived in the present work can reproduce not only the experimental data of elastic scattering angular distributions induced by ^{11}B, ^{12}C, and ^{16}O but also some elastic scattering induced by other heavy-ions.

Keywords: optical potential, elastic scattering, heavy-ion reactions

DOI: 10.1088/1674-1137/abe84f

I. INTRODUCTION

The nucleus-nucleus interaction potential, which includes the short-range attractive and absorptive nuclear potential and long-range repulsive Coulomb potential, has always been a major issue in nuclear physics. The Coulomb interaction between two nuclei is well known, but the nuclear component is much more difficult to describe. Over the last decades, the optical model potential (OMP) has been widely used to describe the nuclear component, and several different potential forms have been proposed to reproduce a large volume of nuclear reaction data [1-3]. In addition to the nuclear reactions induced by light particles, the nuclear reactions between heavy ions can also be described by the optical model [3-6].

Elastic scattering, the simplest nuclear reaction process, is often used to understand more complicated reaction channels [7]. The optical potential parameters extracted by fitting elastic scattering data can be used to obtain information from the nucleus. A large number of systematic optical parameters have been presented as reliable optical potential parameters for reactions of different systems and different incident energies [3]. In this way, one can acquire the optical potential parameters directly without fitting elastic scattering data. Most of these works focus on the reactions induced by light particles such as protons, neutrons, deuterons, and helium-4 [8-11]. Because of the strong Coulomb interaction between heavy-ions, systematic research on the optical potential between heavy ions is substantially more difficult and scarce than research on reactions induced by light particles. However, considerable progress has been made in recent years. Based on the double folding potential and Pauli nonlocality, Chamon et al. [12] proposed the well-known Sã o Paulo potential (SPP). The work provides a systematic description of the realistic nucleus-nucleus interaction, and it can be applied to various reaction systems includ-

Received 30 June 2020; Accepted 15 October 2020; Published online 9 December 2020

* Support by National Key R&D Program of China (2017YFF0106501), Natural Science Foundation of Guangdong China (2016A030310042), Project funded by China Postdoctoral Science Foundation (2019M652999), National Natural Science Foundation of China (11575118, 11605114, 11490563), Continuous Basic Scientific Research Project (WDJC-2019-13), National key Research and Development Program of China (2016YFA0400502)

† E-mail: zhli@ciae.ac.cn
‡ E-mail: hbsun@szu.edu.cn

ing stable and unstable particles. A modified Woods-Saxon potential based on the Skyrme energy-density functional approach was proposed by Wang *et al.* [13, 14] to provide a global description of nucleus-nucleus interactions. Not only elastic scattering but also the fusion barrier and fission barrier of fusion-fission reactions can be described using this potential. By analyzing the angular distributions of ^{6,7}Li elastic scattering from heavy-ions, Xu and Pang proposed a systematic single-folding potential. These systematics can provide a reasonable account of both the elastic scattering and total reaction cross sections [15]. We propose a systematic six-parameter Woods-Saxon potential with fixed imaginary parameters based on the elastic scattering angular distributions induced by ^{12}C [16]. It is not satisfactory for some elastic scattering at energies around the Coulomb barriers or higher than 300 MeV, which may be attributable to the fixed imaginary potential parameters.

In the present work, the Woods-Saxon shape is adopted for both the real and imaginary parts, and the imaginary parameters are also studied as variables. Experimental elastic scattering angular distributions of ^{11}B, ^{12}C, and ^{16}O + heavy-ions are used to extract the optical potential parameters.

II. EXTRACTION OF THE WOODS-SAXON POTENTIAL PARAMETERS

The Woods-Saxon model potential was proposed by Woods and Saxon to approximate the shape of the nuclear component of nucleus-nucleus interactions [17]. Although it is a phenomenological approximation, reactions of different incident energies and different projectile-target combinations can be well reproduced with the six parameters used in the calculations [7].

The six-parameter Woods-Saxon potential contains a real component and an imaginary component and is expressed as

$$V_n(r) = -\frac{V}{1+\mathrm{e}^{(r-R_V)/a_V}} - \frac{\mathrm{i}W}{1+\mathrm{e}^{(r-R_W)/a_W}}, \qquad (1)$$

where V and W are potential depth parameters for the real and imaginary potentials, respectively; $R_i = r_i(A_1^{1/3}+A_2^{1/3})$, in which $i = V, W$, denotes the real and imaginary radius parameters; a_V and a_W respectively refer to the real and imaginary diffuseness; and A_1 and A_2 are the mass numbers of the projectile and target nuclei.

The Coulomb potential is always expressed as

$$V_{\mathrm{C}}(r) = \begin{cases} \dfrac{Z_1Z_2e^2}{2R_{\mathrm{C}}}\left(3-\dfrac{r^2}{R_{\mathrm{C}}^2}\right) & r < R_{\mathrm{C}}, \\ \dfrac{Z_1Z_2e^2}{r} & r > R_{\mathrm{C}}, \end{cases} \qquad (2)$$

where $R_{\mathrm{C}} = r_{\mathrm{C}}(A_1^{1/3}+A_2^{1/3})$ is the radius parameter. It has been proved that theoretical angular distributions are not sensitive to changes in the Coulomb radius [18]. Therefore, a fixed r_{C} equal to 1.0 fm is used throughout the following processes.

In the present work, 27 sets of elastic scattering angular distribution data are adopted to extract the Woods-Saxon potential parameters. The targets range from ^{12}C to ^{209}Bi, and the incident energies range from 25 to 420 MeV. Most of the data are from the National Nuclear Data Center, while the angular distributions of ^{12}C elastic scattering from ^{90}Zr, ^{91}Zr, ^{96}Zr , and ^{116}Sn were measured at the China Institute of Atomic Energy (CIAE), Beijing. Because the optical potential parameters have large ambiguities, several different sets of parameter combinations can reproduce the experimental data well [19]. It has been confirmed that when fitting two or more optical potential parameters at the same time, we easily fall into a minimum trap. In order to study the intrinsic relationship between these parameters, we define more than 1 million sets of parameter combinations of W, R_V, R_W, a_V , and a_W in advance and then use each of them to fit V for all the data. W varies in the range of 10 - 300 MeV by steps of 2 MeV. The geometric parameters of the real and imaginary components are set to the same value, i.e., $r_V = r_W$, and vary between 0.5 and 1.5 fm in increments of 0.01 fm. Finally, $a_V = a_W$ vary between 0.3 and 1.0 fm in increments of 0.01 fm. The analysis process can be divided into four steps:

1) Use all the parameter combinations to fit each elastic scattering dataset with the nuclear reaction code PTOLEMY [20]. In this way, the output V and corresponding χ^2 are obtained for every calculation.

2) Analyze the correlation of χ^2 with the depth, radius, and diffuseness parameters. We find that, for each system, there exists a suitable value of the diffuseness parameter that gives the minimum χ^2. As a typical result, Figure 1 shows χ^2 versus the diffuseness parameter for ^{12}C + ^{90}Zr elastic scattering. However, the depth and radius parameters cannot be extracted in the same way as the diffuseness parameter because there are no best fit values for these parameters. We list the extracted diffuseness for each interaction system in Table 1. The analysis of the diffuseness uncertainties employs the χ^2 envelope method proposed in Ref. [21]. A linear formula for the diffuseness parameter a versus $A_1^{1/3}+A_2^{1/3}$ is summarized in Eq. (3) and shown in Fig. 2; the uncertainties of the slope and intercept are 0.011 and 0.063 fm, respectively. The slope is negative, indicating that as the mass of the system increases, the diffuseness parameter tends to decrease.

$$a_V = a_W = -0.0736(A_1^{1/3}+A_2^{1/3}) + 1.087 \ \text{(fm)}. \qquad (3)$$

3) When the diffuseness parameters are fixed as in

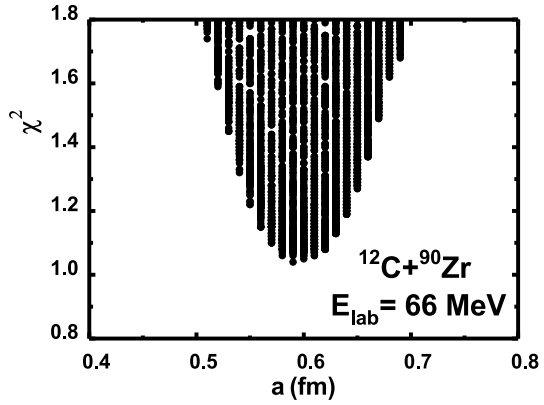

Fig. 1. χ^2 versus the diffuseness parameter for ^{12}C + ^{90}Zr at 66 MeV. Each dot represents a parameter set. It is found that $a = 0.59$ fm corresponds to the minimum χ^2.

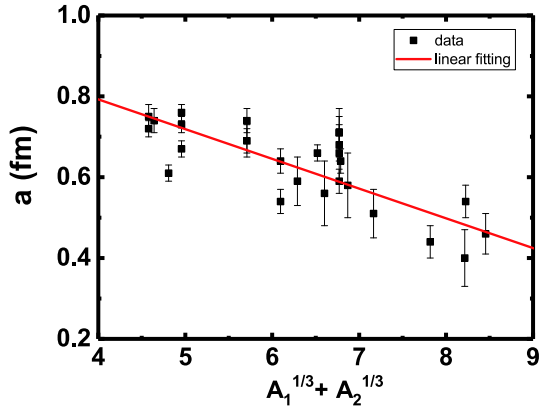

Fig. 2. (color online) The diffusion parameter as a function of $A_1^{1/3}+A_2^{1/3}$.

Table 1. The most suitable diffuseness parameters extracted in the analysis.

Reaction	E_{lab}/MeV	a/fm	Δa/fm
^{11}B+^{58}Ni	25	0.64	0.03
^{11}B+^{58}Ni	35	0.54	0.03
^{12}C+^{12}C	158	0.72	0.02
^{12}C+^{12}C	360	0.75	0.03
^{12}C+^{13}C	127.2	0.74	0.03
^{12}C+^{16}O	76.8	0.61	0.02
^{12}C+^{19}F	40.3	0.67	0.02
^{12}C+^{19}F	50	0.76	0.02
^{12}C+^{19}F	60	0.73	0.02
^{12}C+^{40}Ca	180	0.69	0.03
^{12}C+^{40}Ca	300	0.69	0.04
^{12}C+^{40}Ca	420	0.74	0.03
^{12}C+^{64}Ni	48	0.59	0.06
^{12}C+^{90}Zr	66	0.59	0.03
^{12}C+^{90}Zr	120	0.71	0.04
^{12}C+^{90}Zr	180	0.68	0.04
^{12}C+^{90}Zr	300	0.66	0.07
^{12}C+^{90}Zr	420	0.71	0.06
^{12}C+^{91}Zr	66	0.64	0.03
^{12}C+^{96}Zr	66	0.58	0.08
^{12}C+^{116}Sn	66	0.51	0.06
^{12}C+^{169}Tm	84	0.44	0.04
^{12}C+^{208}Pb	58.9	0.40	0.07
^{12}C+^{209}Bi	87.4	0.54	0.04
^{16}O+^{64}Zn	48	0.66	0.07
^{16}O+^{68}Zn	52	0.56	0.08
^{16}O+^{209}Bi	90	0.46	0.05

Eq. (3), we find a correlation between the depth and radius parameters with the real and imaginary parts, respectively. As an example, χ^2 versus the depth parameters of ^{12}C + ^{90}Zr elastic scattering at 66 MeV is shown in Fig. 3. It is obvious that the curve for V is much steeper than that for W, which indicates that χ^2 is more sensitive to V than to W. Each curve corresponds to a specific radius parameter value, and the correlations of the depth and radius parameter combinations of best fit are as follows:

$$\begin{aligned} V\times\exp(R_V/a_V) &= const1,\\ W\times\exp(R_W/a_W) &= const2. \end{aligned} \tag{4}$$

The values of $const1$ and $const2$ are listed in Table 2. The errors stem from the uncertainties of the diffuseness parameters. Since the radius parameter and diffuseness parameter are the same for the real and imaginary components, the ratio of W to V is equal to the ratio of $const2$ to $const1$.

For most of the nuclear reactions analyzed here, because the incident energies are around or below the Coulomb barrier, the energy dispersion relation between the real and imaginary potentials [22-25] cannot be ignored. Due to the scarcity of energy points around the Coulomb barrier for each system analyzed in the present work, we cannot conduct a detailed study of the energy dispersion relation. We instead propose a rough method to analyze the relationship between the real and imaginary parts near the Coulomb barrier. As the Coulomb barrier is proportional to $Z_1Z_2/(A_1^{1/3}+A_2^{1/3})$, we adopt $E_{\rm lab}\times(A_1^{1/3}+A_2^{1/3})/Z_1Z_2$ as the energy dispersion relation parameter ($EDRP$) to study the energy dependence of the ratio of W to V, as shown in Fig. 4. The trend of W/V versus $EDRP$ has a turning point near $EDRP = 10$. When $EDRP < 10$, the value of W/V decreases rapidly as $EDRP$ decreases. When $EDRP \geqslant 10$, the value of W/V remains relatively stable. We thus determine the expression of W/V as $W/V = (0.0416\pm0.0220)\times EDRP + (0.4124\pm0.0879)$, $EDRP < 10$;

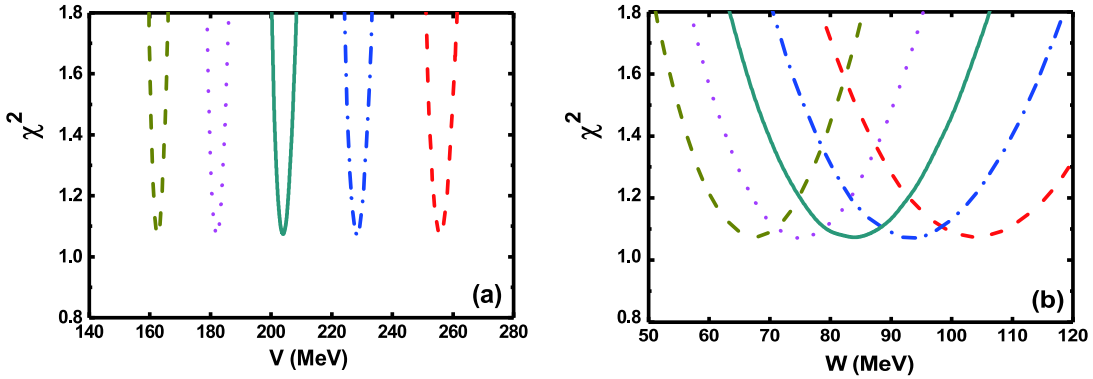

Fig. 3. (color online) χ^2 versus V (a) and W (b) for ^{12}C + ^{90}Zr at 66 MeV. Each curve corresponds to a different radius parameter; the valleys give almost the same χ^2. The radius parameters for each curve from left to right are 1.07 to 1.03 fm, by steps of 0.01 fm. Observe that the curves for V (a) are much steeper than those for W (b).

Table 2. Volume integrals (*Vol*) calculated with SPP, *const*1 , and *const*2 in Eq. (4); the real depth (V) and radius (R) parameters are determined by the Volume integrals and *const*1.

Reaction	$E_{\rm lab}$/MeV	*Vol*/(MeV · fm^3)	*const*1/MeV	*const*2/MeV	V/MeV	R/fm
^{11}B+^{58}Ni	25	418.5	$3.02\times10^{6}\pm1.16\times10^{6}$	$5.79\times10^{5}\pm2.40\times10^{5}$	266.1±34.8	6.00±0.30
^{11}B+^{58}Ni	35	415.6	$2.66\times10^{6}\pm9.88\times10^{5}$	$1.29\times10^{6}\pm5.59\times10^{5}$	277.0±36.0	5.89±0.29
^{12}C+^{12}C	158	416.7	$2.54\times10^{4}\pm8.88\times10^{3}$	$1.90\times10^{4}\pm7.43\times10^{3}$	221.5±54.2	3.56±0.43
^{12}C+^{12}C	360	365.4	$1.86\times10^{4}\pm1.39\times10^{4}$	$1.37\times10^{4}\pm9.93\times10^{3}$	234.4±97.7	3.28±0.82
^{12}C+^{13}C	127.2	422.6	$2.58\times10^{4}\pm1.03\times10^{4}$	$1.89\times10^{4}\pm7.56\times10^{3}$	254.5±70.0	3.49±0.50
^{12}C+^{16}O	76.8	431.4	$5.41\times10^{4}\pm3.74\times10^{4}$	$1.76\times10^{4}\pm1.14\times10^{4}$	240.0±79.9	3.95±0.68
^{12}C+^{19}F	40.3	436.9	$6.66\times10^{4}\pm4.00\times10^{4}$	$4.86\times10^{4}\pm3.55\times10^{3}$	306.8±95.2	3.87±0.60
^{12}C+^{19}F	50	434.1	$7.71\times10^{4}\pm4.99\times10^{4}$	$4.38\times10^{4}\pm3.22\times10^{4}$	267.8±81.5	4.07±0.62
^{12}C+^{19}F	60	431.3	$7.79\times10^{4}\pm277\times10^{4}$	$5.05\times10^{4}\pm1.42\times10^{4}$	263.3±54.8	4.09±0.39
^{12}C+^{40}Ca	180	384.4	$5.90\times10^{5}\pm260\times10^{5}$	$5.70\times10^{5}\pm2.21\times10^{5}$	283.9±51.3	5.10±0.38
^{12}C+^{40}Ca	300	356.3	$4.63\times10^{5}\pm2.00\times10^{5}$	$4.88\times10^{5}\pm2.05\times10^{5}$	336.1±64.9	4.83±0.38
^{12}C+^{40}Ca	420	330.4	$5.53\times10^{5}\pm2.23\times10^{5}$	$5.58\times10^{5}\pm2.07\times10^{5}$	234.5±37.7	5.18±0.34
^{12}C+^{64}Ni	48	409.6	$7.69\times10^{6}\pm4.97\times10^{6}$	$2.96\times10^{6}\pm1.50\times10^{6}$	258.9±44.1	6.43±0.43
^{12}C+^{90}Zr	66	400.9	$4.85\times10^{7}\pm1.21\times10^{7}$	$1.88\times10^{7}\pm6.17\times10^{6}$	266.3±16.8	7.13±0.17
^{12}C+^{90}Zr	120	387.5	$3.83\times10^{7}\pm2.60\times10^{7}$	$1.85\times10^{7}\pm1.15\times10^{7}$	274.4±40.8	6.97±0.40
^{12}C+^{90}Zr	180	376.1	$2.63\times10^{7}\pm1.74\times10^{7}$	$1.32\times10^{7}\pm8.29\times10^{6}$	298.6±43.9	6.70±0.39
^{12}C+^{90}Zr	300	349.1	$2.96\times10^{7}\pm2.01\times10^{7}$	$3.05\times10^{7}\pm2.02\times10^{7}$	260.8±38.9	6.85±0.40
^{12}C+^{90}Zr	420	324.2	$2.06\times10^{7}\pm1.32\times10^{7}$	$1.66\times10^{7}\pm1.08\times10^{7}$	264.5±38.9	6.63±0.39
^{12}C+^{91}Zr	66	400.4	$5.14\times10^{7}\pm3.53\times10^{7}$	$1.80\times10^{7}\pm1.12\times10^{7}$	267.6±36.8	7.15±0.39
^{12}C+^{96}Zr	66	402	$8.90\times10^{7}\pm6.26\times10^{7}$	$2.73\times10^{7}\pm1.71\times10^{7}$	253.7±35.9	7.42±0.40
^{12}C+^{116}Sn	66	397	$2.85\times10^{8}\pm2.09\times10^{8}$	$8.03\times10^{7}\pm5.31\times10^{7}$	273.3±36.1	7.75±0.39
^{12}C+^{169}Tm	84	396.3	$1.08\times10^{10}\pm7.86\times10^{9}$	$6.78\times10^{9}\pm4.88\times10^{9}$	254.3±26.2	8.98±0.34
^{12}C+^{208}Pb	58.9	402.2	$8.95\times10^{10}\pm7.71\times10^{10}$	$5.40\times10^{10}\pm4.68\times10^{10}$	275.6±29.0	9.45±0.35
^{12}C+^{209}Bi	87.4	395.2	$1.14\times10^{11}\pm9.85\times10^{10}$	$3.73\times10^{10}\pm3.03\times10^{10}$	262.0±14.5	9.56±0.35
^{16}O+^{64}Zn	48	409.3	$1.98\times10^{7}\pm1.09\times10^{7}$	$8.12\times10^{6}\pm4.36\times10^{6}$	303.8±42.4	6.73±0.36
^{16}O+^{68}Zn	48	408.6	$3.96\times10^{7}\pm2.31\times10^{7}$	$2.39\times10^{7}\pm1.33\times10^{7}$	270.6±36.2	7.15±0.36
^{16}O+^{209}Bi	90	394.9	$1.15\times10^{12}\pm1.04\times10^{12}$	$1.40\times10^{7}\pm1.25\times10^{1}2$	284.6±28.0	10.28±0.35

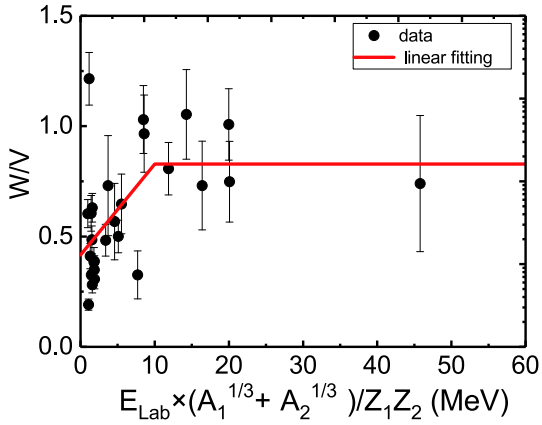

Fig. 4. (color online) Value of W/V versus $E_{\rm lab}\times(A_1^{1/3}+A_2^{1/3})/Z_1Z_2$. The dots represent the value for each system. W/V decreases sharply when $E_{\rm lab}\times(A_1^{1/3}+A_2^{1/3})/Z_1Z_2 <$ 10 and remains relatively stable when $E_{\rm lab}\times(A_1^{1/3}+A_2^{1/3})/Z_1Z_2 \geqslant 10$. The red line is a simple linear fit to describe the behavior of W/V.

$W/V = (0.8284 \pm 0.1321)$, $EDRP \geqslant 10$.

4) The volume integral is considered to be a reliable physical quantity for describing the total strength of a potential [26, 27]; it is expressed as

$$J_V = \frac{4\pi}{A_1\,A_2}\int V_n(r)r^2\,{\rm d}r. \tag{5}$$

The SPP can describe the realistic potential successfully [12, 28], and it is adopted to calculate the volume integrals for every system in this work. The depth and radius parameters are determined by requiring that they satisfy Eq. (4) [with a determined by Eq. (3)] and their corresponding J_V-values are the same as those given by the SPP systematics. The calculated volume integrals and depth and radius parameters are shown in Table 2 and in Figs. 5, 6, and 7, respectively.

In Fig. 5, it is evident that the volume integrals of the various systems are relatively close and that they decrease slightly as the incident energy increases. The depth of the real part of each system exhibits system independence and an insignificant energy dependence. The variations in the real depth induced by the incident energy are less than 10 MeV for all systems, and the theoretical angular distributions rarely change. An average value of 268.7 ± 24.1 MeV is thus adopted for the depth, as shown in Fig. 6. The analysis of the radius parameters is shown in Fig. 7, where we find that the linear expression with $A_1^{1/3}+A_2^{1/3}$ describes the trend of the radius parameter very well. The expressions of the depth and radius parameters are shown in Eq. (6). Using the expressions for the optical potential parameters in Eq. (3) and Eq. (6), *const*1 and *const*2 can be calculated for all systems, the results of which are plotted in Fig. 8.

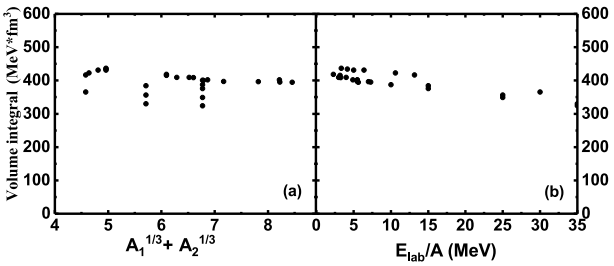

Fig. 5. Volume integrals versus $(A_1^{1/3}+A_2^{1/3})$ (a) and incident energy (b). The volume integrals of the different systems are similar, and they decrease slightly as the incident energy increases.

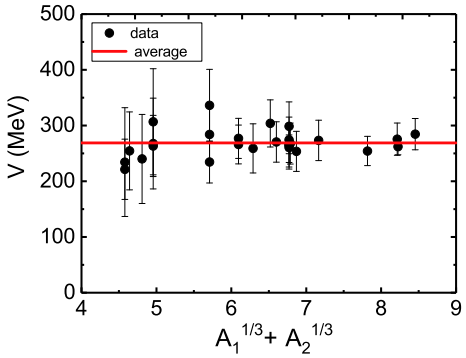

Fig. 6. (color online) Depth of the real part determined by *const*1 and the volume integral. The values show system independence.

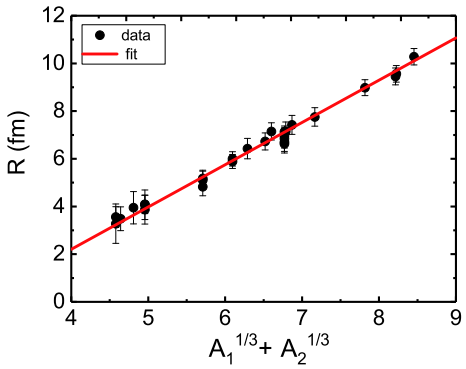

Fig. 7. (color online) Radius parameters determined by *const*1 and the volume integral. There is a strong linear relationship between the radius parameter and $(A_1^{1/3}+A_2^{1/3})$.

$$\begin{aligned}
V &= (268.7 \pm 24.1)\ \ ({\rm MeV}),\\
W/V &= \begin{cases} 0.0416\times EDRP + 0.4124 & EDRP < 10,\\ 0.8284 & EDRP \geqslant 10,\end{cases}\\
R_V &= R_W = (1.772 \pm 0.039)\times(A_1^{1/3}+A_2^{1/3})\\
&\quad -(4.881 \pm 0.256)\ \ ({\rm fm}),\\
EDRP &= E_{\rm lab}\times(A_1^{1/3}+A_2^{1/3})/Z_1Z_2.
\end{aligned} \tag{6}$$

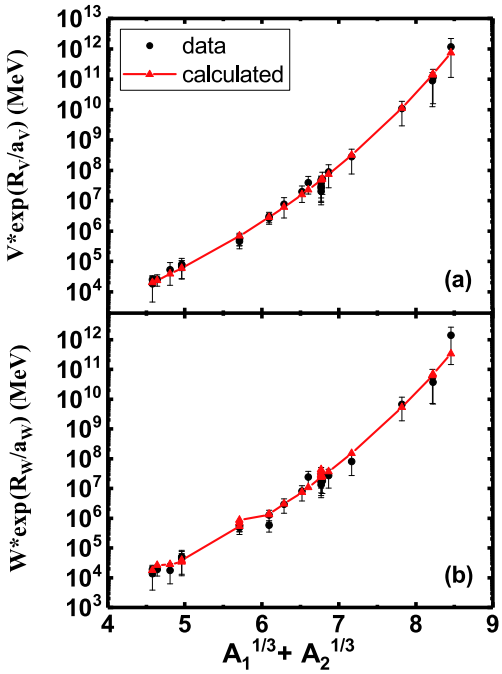

Fig. 8. (color online) Values of *const*1 (a) and *const*2 (b) in Eq. (4) versus $A_1^{1/3}+A_2^{1/3}$ for each reaction. The values of *const*1 and *const*2 increase sharply as $A_1^{1/3}+A_2^{1/3}$ increases. The dots with error bars represent the data, and the red triangles denote the results calculated by adopting the formulas in Eqs. (3) and (6). The theoretical points are connected by the red curves to describe the trend of *const*1 and *const*2.

III. VERIFICATION OF THE SYSTEMATIC POTENTIAL

The systematics of the Woods-Saxon parameters extracted in the present work are checked using various elastic scattering data. The systematics derived by Wang *et al.* [13, 14] and Xu *et al.* [15] are also employed to calculate angular distributions for comparison. The results can be seen in Figs. 9-13.

The current systematic potential parameters can reproduce the experimental data very well, not only for the elastic scattering induced by ^{11}B, ^{12}C , and ^{16}O but also for other systems, such as ^{28}Si, ^{32}S, and ^{40}Ca + nucleus. For most of the systems, our results yield a description similar to those of Xu *et al.* [15] and Wang *et al.* [13, 14]. For some scattering systems, especially for relatively light systems, such as ^{12}C + ^{12}C at 158.8 MeV and 360 MeV (Fig. 9), ^{12}C + ^{13}C at 127.2 MeV (Fig. 9), and ^{11}B + ^{58}Ni at 25 MeV (Fig. 13), the present systematic results are even better.

IV. CONCLUSION

The elastic scattering angular distributions of ^{11}B, ^{12}C, and ^{16}O + heavy-ions at incident energies between 2.3 and 35 A MeV were fitted with the six-parameter Woods-Saxon potential. We obtained χ^2 for each calculation to find the best-fit parameter combinations. The diffuseness parameter was determined first, followed by the relationship with $A_1^{1/3}+A_2^{1/3}$. Using the formula for the diffuseness parameter, the ratio of the imaginary depth to the real depth was obtained, and the correlation between the depth and radius parameters was found. With the limitation of the volume integrals calculated using SPP, the values of the depth and radius parameters of various systems were determined. Because the real depth exhibits

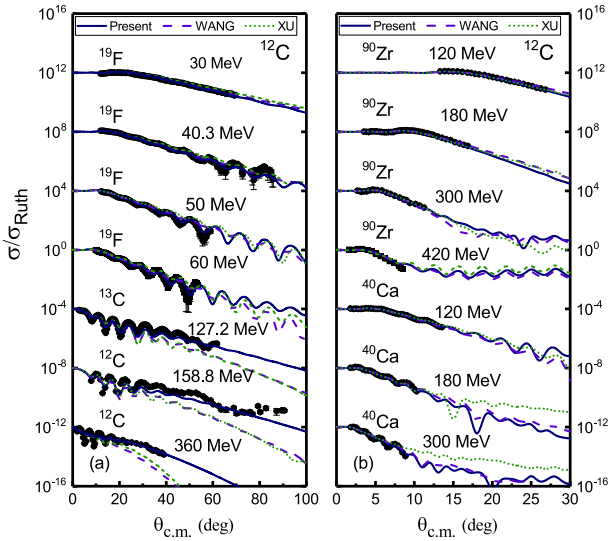

Fig. 9. (color online) Comparison of the differential cross sections from the experimental data and theoretical calculations. The solid curves are calculated with the systematics summarized in this work. The results of Xu *et al.* [15] (dashed line) and Wang *et al.* [13, 14] (short dashed line) are also shown. The different data sets are offset by factors of 10^4. The experimental data are from Refs. [29-33].

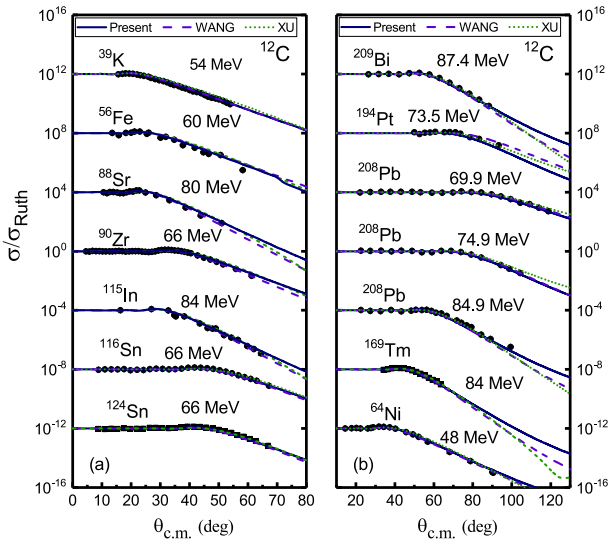

Fig. 10. (color online) Same as Fig. 9 but with different targets. The experimental data are from Refs. [34-42].

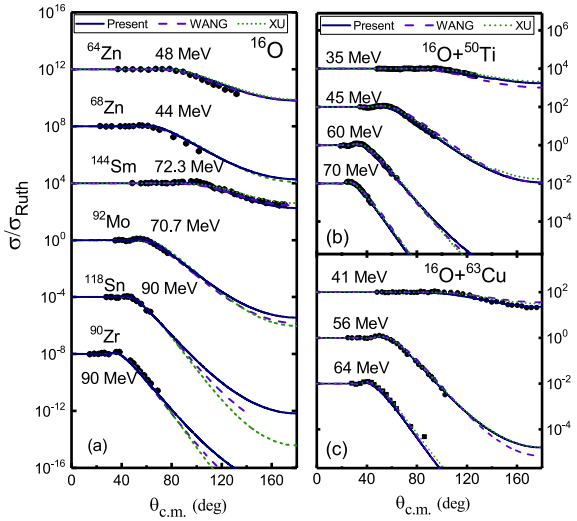

Fig. 11. (color online) Elastic scattering angular distributions of ^{16}O + heavy-ions. The experimental data are from Refs. [43-49].

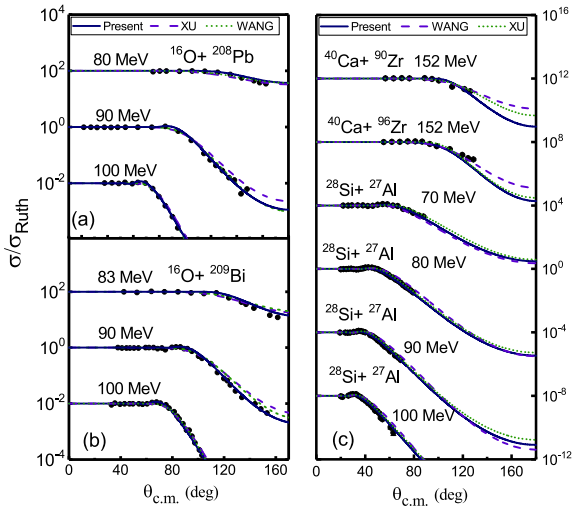

Fig. 12. (color online) Elastic scattering angular distributions of ^{16}O + heavy-ions in panels (a) and (b) and ^{40}Ca+^{90,96}Zr and ^{28}Si+^{27}Al in panel (c). The experimental data are from Refs. [50-53].

system independence and ignorable energy dependence,

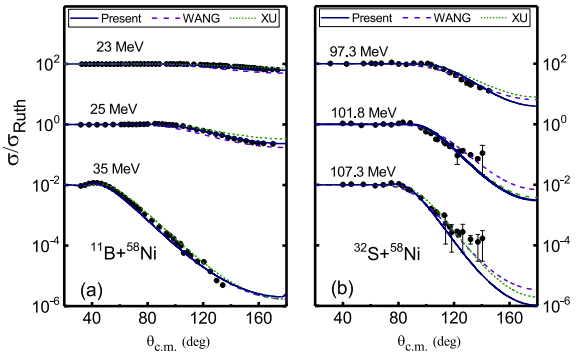

Fig. 13. (color online) Elastic scattering angular distributions of ^{11}B+^{58}Ni at different incident energies in panel (a) and ^{32}S+^{58}Ni at different incident energies in panel (b). The different data sets are offset by factors of 10^2. The experimental data are from Refs. [54, 55].

the average value was adopted for all systems. The values of W/V show strong energy dependence when the incident energy is below or around the Coulomb barrier. The radius parameters have a strong linear relationship with $A_1^{1/3}+A_2^{1/3}$, and the expression was fitted. The systematic potential parameters summarized in the present work reproduce various interaction systems induced by ^{11}B, ^{12}C, and ^{16}O well and can also reproduce elastic scattering induced by other heavy ions, such as ^{28}Si, ^{32}S, and ^{40}Ca + nucleus.

Nevertheless, the present work is not fully satisfactory. For some heavy systems, such as ^{40}Ca+^{96}Zr at incident energies of 152 MeV [52], our result is not quite satisfactory. More detailed studies are needed to analyze the relevant parameters, such as isospin.

It is difficult to directly extract the optical potential between some heavy ions, especially those between unstable nuclei. Nonetheless, the systematic study of optical potential parameters in these situations is particularly important. Although there have been some studies on the nuclear-nuclear interaction potential between heavy ions, these works have system limitations; that is, some systems are reproduced well, while others are not. Therefore, further research in this area is still needed.

References

[1] C. J. Lin, H. M. Jia, H. Q. Zhang *et al.*, Phys. Rev. C **79**, 064603 (2009)

[2] M. Y. H. Farag, E. H. Esmael, and H. M. Maridi, Phys. Rev. C **90**, 034615 (2014)

[3] W. H. Dickhoff and R. J. Charity, Prog. Part. Nucl. Phys. **105**, 252 (2018)

[4] N. T. Zhang, Y. D. Fang, P. R. S. Gomes *et al.*, Phys. Rev. C **90**, 024621 (2014)

[5] V. Avrigeanu and M. Avrigeanu, Phys. Rev. C **91**, 064611 (2015)

[6] T. Furumoto, Y. Sakuragi, and Y. Yamamoto, Prog. Theor. Phys. Supplement **196**, 219 (2012)

[7] M. A. G. Alvarez, L. C. Chamon, M. S. Hussein *et al.*, Nucl. Phys. A **723**, 93 (2003)

[8] F. G. Perey, Phys. Rev. C **131**, 745 (1963)

[9] J. M. Lohr and W. Haeberli, Nucl. Phys. A **723**, 381 (1974)

[10] J. Rapaport, V. Kulkarni, and R. Finlay, Nucl. Phys. A **330**, 15 (1979)

[11] A. Kumar, S. Kailas, S. Rathi *et al.*, Nucl. Phys. A **776**, 105 (2006)

[12] L. C. Chamon, B. V. Carlson, L. R. Gasques *et al.*, Phys. Rev. C **66**, 014610 (2002)

[13] N. Wang, K. Zhao, W. Scheid *et al.*, Phys. Rev. C **77**,

014603 (2008)
[14] N. Wang and W. Scheid, Phys. Rev. C **78**, 014607 (2008)
[15] Y. P. Xu and D. Y. Pang, Phys. Rev. C **87**, 044605 (2013)
[16] L. Gan, Z. H. Li, H. B. Sun *et al.*, Sci. China-Phys. Mech. Astron. **60**, 082013 (2017)
[17] R. D. Woods and D. S. Saxon, Phys. Rev. **95**, 577 (1954)
[18] J. E. Poling, E. Norbeck, and R. R. Carlsoni, Phys. Rev. C **13**, 648 (1976)
[19] G. Igo, Phys. Rev. **115**, 1665 (1959)
[20] M. H. Macfarlane and S. C. Pieper, A. PTOLEMY, Argonne National Laboratory, unpublished, 1978
[21] M. Evers, M. Dasgupta, D. J. Hinde *et al.*, Phys. Rev. C **78**, 034614 (2008)
[22] G. R. Satchler, Phys Lett. B **58**, 408 (1975)
[23] M. A. Nagarajan, C. C. Mahaux, and G. R. Satchler, Phys Rev. Lett. **54**, 1136 (1985)
[24] B. R. Fulton, D. W. Banes, J. S. Lilley *et al.*, Phys Lett. B **162**, 55 (1985)
[25] L. Yang, C. J. Lin, H. M. Jia *et al.*, Phys Rev. Lett. **119**, 042503 (2017)
[26] H. Feshbach, Annual Review of Nuclear Science **8**, 49 (1958)
[27] S. J. Waldecker, C. Barbieri, and W. H. Dickhoff, Phys. Rev. C **84**, 34616 (2011)
[28] A. S. Freitas, L. Marques, X. X. Zhang *et al.*, Braz. J. Phys. **46**, 120 (2016)
[29] T. Tachikawa, N. Kato, H. Fujita *et al.*, Nucl. Phys. A **484**, 125 (1988)
[30] T. Al-Abdullah, F. Carstoiu, X. Chen *et al.*, Phys. Rev. C **81**, 035802 (2010)
[31] S. Kubono, K. Morita, M. H. Tanaka *et al.*, Phys. Lett. B **127**, 19 (1983)
[32] M. Buenerd, A. Lounis, J. Chauvin *et al.*, Nucl. Phys. A **424**, 313 (1988)
[33] C. C. Sahm, T. Murakami, J. G. Cramer *et al.*, Phys. Rev. C **34**, 2165 (1986)
[34] C. W. Glover, K. W. Kemper, Parks L A *et al.*, Nucl. Phys. A **337**, 520 (1980)
[35] H. S. Patel, B. Srinivasan, B. J. Roy *et al.*, Pramana-J. Phys. **51**, 433 (1998)
[36] G. Ingold, H. G. Bohlen, M. Clover *et al.*, Z.Phys. A-Atoms and Nuclei **305**, 135 (1982)
[37] B. J. Roy, M. G. Betigeri, M. L. Jhingan *et al.*, Nucl. Phys. A **564**, 271 (1993)
[38] S. Sodaye, K. Sudarshan, B. S. Tomar *et al.*, Eur. Phys. J. A **564**, 371 (2002)
[39] A. Shrivastava, S. Kailas, A. Chatterjee *et al.*, Phys. Rev. C **63**, 054602 (2001)
[40] S. Santra, P. Singh, S. Kailas *et al.*, Phys. Rev. C **64**, 024602 (2001)
[41] S. Santra, P. Singh, S. Kailas *et al.*, Phys. Rev. C **60**, 034611 (1999)
[42] A. Cunsolo, M. C. Lemaire, M. C. Mermaz *et al.*, Phys. Rev. C **10**, 180 (1974)
[43] C. F. Tenreiro, J. C. Acquadro, N. Liguori *et al.*, Study of the ^{16}O+ $^{64,\ 66,\ 68}$Zn reactions: fusion and elastic scattering. No. IFUSP-P-710. Brazil, Sao Paulo Univ., 1988. 11
[44] D. Abriola, D. DiGregorio, J. E. Testoni *et al.*, Phys. Rev. C **39**, 546 (1989)
[45] K. E. Rehm, H. J. Körner, M. Richter *et al.*, Phys. Rev. C **12**, 1945 (1975)
[46] S. Saha, S. K. Mandal, M. B. Chatterjee *et al.*, Pramana-J. Phys. **53**, 553 (1999)
[47] V. Jha, B. J. Roy, A. Chatterjee *et al.*, Eur. Phys. J. A **19**, 347 (2004)
[48] J. C. Werner, L. A. S. Leal, M. G. Munhoz *et al.*, Nucl. Phys. A **781**, 342 (2007)
[49] R. Lichtenthäler, D. Pereira, and L. C. Chamon, Phys. Rev. C **50**, 3033 (1994)
[50] F. Videbaek, R. B. Goldstein, L. Grodzins *et al.*, Phys. Rev. C **17**, 954 (1977)
[51] P. Singh, S. Kailas, A. Chatterjee *et al.*, Nucl. Phys. A **555**, 606 (1993)
[52] G. Montagnoli, S. Beghini, F. Scarlassara *et al.*, J. Phys. G: Nucl. Part. Phys. **23**, 1431 (1997)
[53] S. K. Charagi, S. K. Gupta, M. G. Betigeri *et al.*, Phys. Rev. C **48**, 1152 (1993)
[54] N. N. Deshmukh, V. Guimarães, E. Crema *et al.*, Phys. Rev. C **92**, 054615 (2015)
[55] A. M. Stefanini, A. Tivelli, G. Montagnoli *et al.*, Phys. Rev. C **41**, 1018 (1990)